A sub-sampled approach to extremely low-dose STEM

Cite as: Appl. Phys. Lett. **112**, 043104 (2018); https://doi.org/10.1063/1.5016192
Submitted: 16 November 2017 . Accepted: 29 December 2017 . Published Online: 24 January 2018

A. Stevens, L. Luzi, H. Yang, L. Kovarik, B. L. Mehdi, A. Liyu, M. E. Gehm, and N. D. Browning

A sub-sampled approach to extremely low-dose STEM

A. Stevens,[1,2,a)] L. Luzi,[3] H. Yang,[4] L. Kovarik,[5] B. L. Mehdi,[5,6] A. Liyu,[5] M. E. Gehm,[2] and N. D. Browning[5,6]
[1]*OptimalSensing, Southlake, Texas 76092, USA*
[2]*Duke University, ECE, Durham, North Carolina 27708, USA*
[3]*Rice University, ECE, Houston, Texas 77005, USA*
[4]*Lawrence Berkeley National Laboratory, Berkeley, California 94720, USA*
[5]*Pacific NW National Laboratory, Richland, Washington 99354, USA*
[6]*University of Liverpool, Materials Engineering, Liverpool L69 3GH, United Kingdom*

(Received 16 November 2017; accepted 29 December 2017; published online 24 January 2018)

The inpainting of deliberately and randomly sub-sampled images offers a potential means to image specimens at a high resolution and under extremely low-dose conditions (≤ 1 e$^-$/Å^2) using a scanning transmission electron microscope. We show that deliberate sub-sampling acquires images at least an order of magnitude faster than conventional low-dose methods for an equivalent electron dose. More importantly, when adaptive sub-sampling is implemented to acquire the images, there is a significant increase in the resolution and sensitivity which accompanies the increase in imaging speed. We demonstrate the potential of this method for beam sensitive materials and *in-situ* observations by experimentally imaging the node distribution in a metal-organic framework. *Published by AIP Publishing.*
https://doi.org/10.1063/1.5016192

The development of aberration correctors for scanning transmission electron microscopes (STEMs)[1] has led to a spatial resolution limit better than 0.5 Å for images of stable inorganic crystalline samples. Accompanying this high level of spatial resolution is a simultaneous increase in image sensitivity which is primarily caused by the increased beam current in the sub-angstrom electron probe used to form the image.[2] While this is incredibly beneficial for achieving an atomic resolution in analytical methods such as electron energy loss spectroscopy (EELS)[3] and energy dispersive X-ray spectroscopy (EDS),[4] the high beam current (typically resulting in a dose on the sample that is in excess of 10^5–10^6 e$^-$/Å^2) drastically reduces the number of samples that are stable under these standard illumination conditions. The key to expanding the applicability of high resolution STEM to beam sensitive materials such as inorganic-organic hybrids,[5] porous materials,[6] and catalysts[7] or *in-situ* observation of dynamic materials processes[8] is the ability to extend the established imaging functionality to much lower electron doses.

The concept of low-dose imaging is well known in transmission electron microscopy (TEM) for structural biology, with dose thresholds for most samples being defined at 10 e$^-$/Å^2 over 30 years ago.[9] In fact, this dose sensitivity, coupled with a need for high contrast at low spatial frequencies, is one of the major reasons why aberration corrected TEM[10] is still not a standard method in structural biology. In contrast, the major advance in the resolution for highly beam sensitive biological materials has come in the last five years with the widespread use of direct detection cameras,[11,12] where the higher sensitivity and increased speed of the camera have allowed high resolution images to be acquired at lower dose. The materials science branch of electron microscopy has used these direct detection cameras primarily for *in-situ* analysis,[13] but more recently observations of metal-organic frameworks (MOFs) have shown the advantage of such cameras for low-dose imaging of hybrid materials.[14]

Although direct detection has been momentous for structural biology and is beginning to have an impact on materials science, it does not provide imaging advantages for all types of samples (and still has challenges for structural biology at the highest resolution limits). First and foremost, the image being collected on the direct detector is a phase contrast image and in the case of biological samples must be highly defocused to image all spatial frequencies in the sample (or be imaged with a phase plate). Phase contrast images are also sensitive to thickness effects, and under most conditions for inorganic samples cannot be intuitively interpreted without simulations (this factor is less important for structural biology but very important for beam sensitive inorganic materials and organic-inorganic composites). This is where the physics of Z-contrast[15] and Annular Bright Field (ABF)[16] STEM imaging have shown important advantages. The incoherent nature of the imaging process provides an intuitive contrast interpretation across all spatial frequencies in the image and works for sample thicknesses of up to $\sim 1\,\mu$m. Furthermore, by calibrating the detector, the image can be quantified directly with atomic precision[17] and scan distortions can be removed to obtain picometer sensitivity[18] in structural images. If we can obtain Z-contrast/ABF images under extremely low-dose conditions, then the approach will synergize the benefits of the STEM contrast mechanisms with the established speed and sensitivity of the direct detectors (this does not mean that low-dose STEM can replace direct detection for all applications, but for cases where Z-contrast or ABF imaging have a benefit, novel low-dose imaging approaches could greatly increase the number of samples that can be observed).

The traditional means of decreasing dose in the STEM is to scan faster (lower dose from a reduced pixel dwell

a)Electronic mail: andrew@optimalsensing.com

time) or reduce the gun extraction voltage (reducing the number of electrons emitted). Both methods experience difficulties in an aberration corrected microscope; to get a low enough dose, either the scan speed exceeds the stability of the scan coils or the reduced extraction voltage misaligns the corrector (the beam cross-overs are changed). Compressive sensing (and related techniques such as inpainting) offers an alternative approach that avoids these limitations. Compressive sensing utilizes the concept that images/data can be well represented in a much sparser form using a suitable basis set and that this sparse form can be fully recovered from a measurement that has a much lower sampling than the conventional acquisition (hence lowering the number of pixels and dose in an image while increasing speed). The theory of compressive sensing[19,20] is now widely applied in many fields. In electron microscopy, compressive sensing has been applied recently for dose reduction in tomography[21] and video rate enhancement[22] and has been proposed as a method for the reduction of dose in STEM imaging.[23]

In this letter, a specific kind of compressive sensing—inpainting is examined as a method for dose reduction. Inpainting can be thought of as an image processing technique to *fill-in* missing data. In the most general form, the pixels are missing arbitrarily, but here the pixels are missing according to a binary random process. The design of the missingness of the pixels is an important consideration for hardware development[24] and guaranteeing recovery of the missing data.[25] The first simulation in this letter examines the equivalence of "conventional" extremely low-dose STEM imaging and inpainting. Second, experimentally collected low-dose and sub-sampled data are used to further justify this equivalence. Third, a reconstruction of experimentally sub-sampled data of a MOF is shown to illustrate the efficacy of sub-sampling on beam sensitive materials. Finally, an adaptive sub-sampling approach is proposed and shown to reduce dose by an order of magnitude below low-dose and sub-sampled STEM in simulation. Several different specimens are used in this letter to reinforce the generality of compressive sensing. Figures consolidating the presented results are shown in the supplementary material.

To determine the optimum approach to inpainting for high-magnification STEM (i.e., the level of dose/sub-sampling that produces the best images), we first compare the results of sub-sampling with a fully sampled conventional low-dose image in simulation. Figure 1 shows simulations of Z-contrast images for ZnSe, which is a standard test sample for atomic resolution STEM (similar results for GaAs are shown in the supplementary material). ZnSe and GaAs are important benchmarks because they have low Z-contrast. These images were simulated using the multi-slice frozen phonon image simulation method in QSTEM.[26] A specimen thickness of 10 nm was used for these simulations. The primary beam energy of the microscope was set to 200 keV. The probe-forming convergence semi-angle was 22 mrad, and the annular dark field (ADF) detector collection angle was 75–300 mrad. A probe source size of 0.6 Å was used, and the image pixel size was 0.2×0.2 Å. To simulate low-dose imaging conditions, each pixel is corrupted with Poisson noise consistent with the mean value predicted by the simulation at the corresponding dose. We note at this

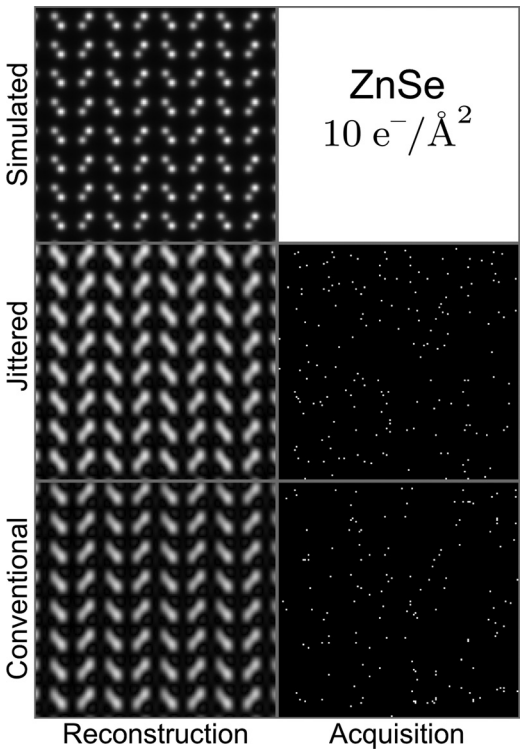

FIG. 1. Representative reconstructions for a dose of $10\,e^{-}/Å^{2}$. The acquisition images have white pixels for electron counts greater than 0. Resolution and contrast metrics are shown in Table I. About 1% of the acquisition pixels detect an electron.

point that there is no requirement for these methods that the sample is crystalline, and the use of sub-sampling to reconstruct non-periodic images has been demonstrated previously.[23] Here, we use a standard sample used to test the resolution of microscopes to make the discussion of sub-sampling more familiar.

The images shown in Fig. 1 illustrate a comparison between the conventional low-dose acquisition strategy (lowering the beam current and/or scanning faster) and the sub-sampling strategy of putting the dose into a few randomly selected pixels. In this example of the sub-sampling approach, 10% of the pixels are used, and the dose is kept consistent with the fully sampled image by increasing the Poisson mean in each sampled pixel by the fraction of sub-sampling (i.e., the sub-sampled dose in a pixel is 10× the dose in a pixel of the fully sampled image, making the total dose the same). In both acquisition images, about 1% of the pixels achieve 1 or more electron counts due to the extremely low dose. The reconstructed images for each sampling strategy use the same algorithm. First, the Fourier transform (FT) is computed. Next, a punctured median filter is used to find the peak and filter-out non-peak regions in the magnitude image. Finally, the magnitude beyond a maximum spatial frequency is set to zero, and the inverse transform gives the reconstructed image.

To determine the overall resolution and sensitivity of the images, the resolution and contrast can be calculated using standard STEM metrics[27] (a ratio estimator is also applied[28]) Because of the randomness in the sub-sampling and application of Poisson noise, an ensemble of 200 reconstructions were performed at each dose. The noise and

random sampling is different for each reconstruction. The average reconstructed resolution for doses in the range of 0.1–100 $e^-/Å^2$ is shown in Fig. 2. In addition, Z-contrast and the probability of obtaining an atomic resolution image are shown in the supplementary material along with the results for a GaAs specimen. Resolution is defined as the distance along the line between the peaks from the lower peak and the first point at 81% intensity of the peak (when the trough is greater than 81%, the peaks are not resolved). As can be seen from Fig. 2, at doses above ~50 $e^-/Å^2$, the resolution of each method is consistent with high dose imaging. At lower doses, deliberate random sub-sampling and conventional low-dose sampling produce approximately the same resolution and contrast. Note that just as any other image processing technique, inpainting can introduce artifacts, such as over-smoothing (reduced resolution).[29] These artifacts are avoided by exploiting the periodicity of the specimen (i.e., enforcing a sparse FT).

The exemplar reconstructions in Fig. 1 and resolution metrics in Fig. 2 provide key intuitive insights into the nature of low-dose imaging in the STEM. Notably, at extremely low-doses, conventional low-dose sensing produces a *de-facto* sub-sampling—99% of the pixels do not contain any scattered electrons. Importantly, however, this unplanned sub-sampling in conventional low-dose imaging causes an unwanted "slow-down" in image acquisition and "wasted" electron dose. Since the deliberate sub-sampling only illuminates 10% of the pixels, the acquisition time is decreased by an order of magnitude (and by eliminating settling time after flyback at the end of each scan line, the reduction in acquisition time is even greater). Furthermore, because the pixels that are illuminated contain 10× the electron dose, there is a greater probability of there being scattering into the detector from those locations, reducing the amount of dose that is simply wasted by not reaching the detector. These results indicate that inpainted reconstructions can improve all forms of low-dose images, but the largest advantage comes with the use of deliberately sub-sampled images.

The deliberately sub-sampled acquisition described above can be demonstrated in practice by the reconstructions from a NiTi oxide sample at varying levels of sub-sampling (Fig. 3). Here, the sub-sampling uses a line-hopping approach rather than the optimum "jittered" sampling[25] shown in Fig. 1. The line-hopping approach is a mechanism to approximate the random sub-sampling without exceeding the hysteresis limits of the electromagnetic scan coils of the JEOL ARM

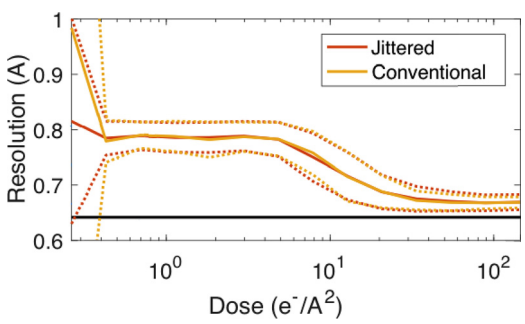

FIG. 2. The plot shows the mean resolution (solid) ± 1 std. deviation (dotted) and actual resolution (solid black).

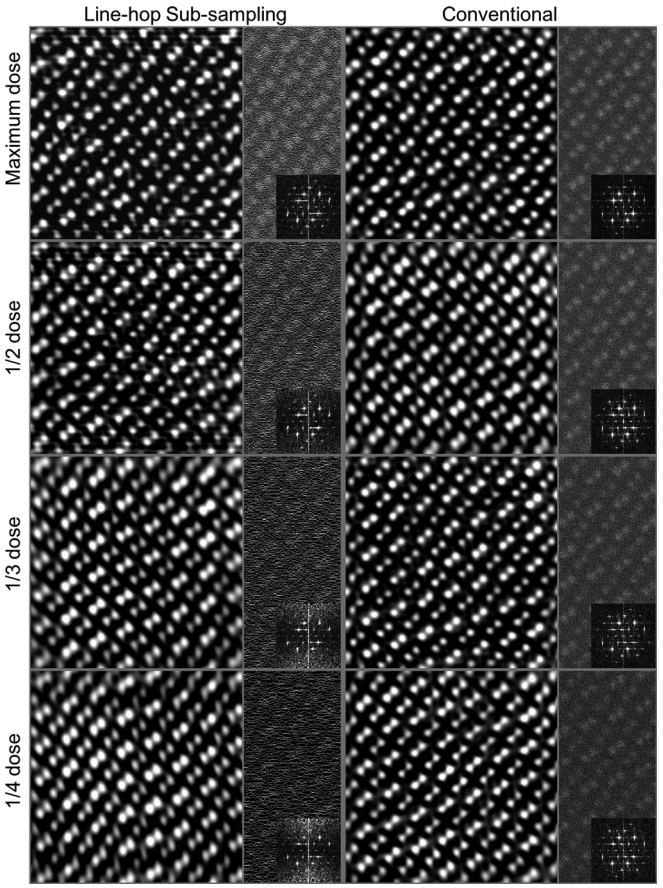

FIG. 3. Reconstruction of real acquisitions of $NiTiO_3$. This agrees with the conventional vs. jittered simulation—all reconstructions are of atomic resolution. The *acquisition* and FT are shown on the right of the reconstructions. Left: line-hop sub-sampled at 50%, 25%, 12.5%, and 6.25%, at a dwell time of 60 μs. Right: conventional, dwell times of 30, 15, 7.5, and 3.75 μs. The same algorithm parameters were used for every reconstruction; by tuning the parameters, better quality can be achieved.

microscope used to acquire these images.[24] This hysteresis limit means that it is not possible in the current system to randomly jump to any point in the image. Instead, the scan moves uniformly in the *x*-direction while moving over a defined pixel range randomly in the *y*-direction (for example, to get 10% scanning, the beam can move randomly −1, 0, +1 pixels over a 10 pixel range). As can be seen in Fig. 3, the sub-sampling approach again produces an equivalent sampling to the low-dose method. Interestingly, the image shows a "missing wedge" of data in the Fourier transform caused by the inability of the line hopping to sample completely randomly in the *y*-direction. This constrained *y*-movement limits the resolution in this case since the pixel size (i.e., random movement) is the same order of magnitude as the structural feature being imaged (it is not possible to increase the magnification to decrease the pixel size or oversample the atom locations as both would increase the dose beyond stability conditions). These results demonstrate that the sub-sampling method can have a significant effect on the reconstruction of the result. Ideally, a fast electrostatic scan generator for a microscope would permit scanning any pixel location and quickly adapting the scan with negligible hysteresis.[30,31]

Fortunately, it is possible to test line-hopping using a beam-sensitive sample with larger dimensions. MOFs[32,33] are bottom-up constructed samples consisting of inorganic

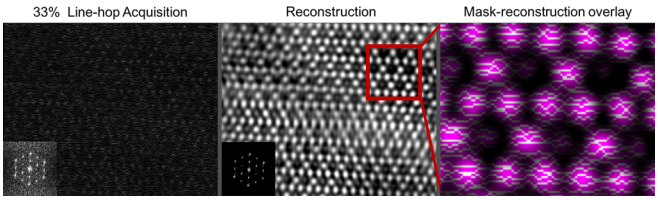

FIG. 4. Reconstruction of a sub-sampled line-hop acquisition from an NU-1000 (Zr_6O_x) MOF. The distortions are caused by synthesis/preparation. The left panel shows a magnified overlay of the scan-lines (white) and the nodes (purple).

nodes separated by organic linkers. The nodes themselves are constructed from oxides containing ∼10 atoms and are ∼1 nm in size. The organic linkers are several nanometers long and can be used to order the nodes in a lattice. Figure 4 shows a sub-sampled acquisition and reconstruction of an NU-1000 MOF[34] with Zirconia nodes which is imaged with 33% line-hopping. The bottom of Fig. 4 illustrates why the MOF structure can be imaged using line-hopping (each node is crossed by several line-hopped scans).

These results have shown that sub-sampling can increase the speed of imaging and if the hysteresis in the scan can be overcome by an electrostatic deflector, tailoring the feature size, or rotating the electron scan between frames, huge gains in speed are also possible. However, we can also potentially increase the resolution and sensitivity of the images that are obtained by "adapting" the sub-sampling to the structure that we are trying to image. Figure 5 shows the result of an adaptive sampling strategy, which begins with an initial Cartesian jittered random sub-sampling, and then, new scans are adapted to sample the regional maxima identified in the previous scan. Each scan collects pixels that have not been previously collected (further details are given in the supplementary material). Such an adaptive approach has the effect of putting the dose in the expected atom column locations. As can be seen from the detailed comparison of the results from the conventional low-dose image, the deliberately sub-sampled (jittered image) and the adaptively sub-sampled image shown in Table I, adaptive sampling maintains the advantages of sub-sampling but could also improve resolution (see supplementary material for comparison figures). Figure 6 shows further that at 1 $e^-/Å^2$, we would expect to recover an atomic resolution image of ZnSe about 50% of the time using adaptive sensing, but conventional and jittered sampling should not be expected to obtain atomic resolution images. The reason for this is that the sub-sampled dose can be used initially to recover a lower resolution image, and then, this image can be used to sample pixels

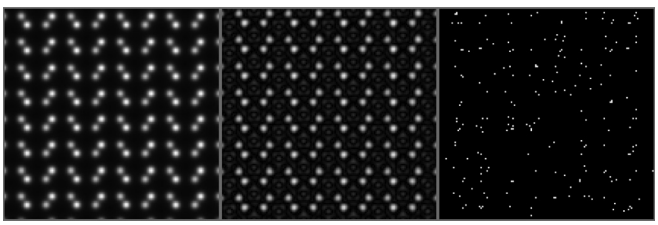

FIG. 5. Adaptive reconstruction of ZnSe at 10 $e^-/Å^2$. Left to right: Simulated, adaptive reconstruction, acquired image after the final adaptive sample.

TABLE I. Resolution and contrast metrics for the images shown in Figs. 1 and 5. For ZnSe, jittered and conventional (convl.) resolutions are inter-dumbbell (not atomic).

Material	GaAs 10 $e^-/Å^2$		ZnSe 10 $e^-/Å^2$	
Method	Res. (Å)	Contrast	Res. (Å)	Contrast
Simulated	0.6115	1.115	0.6414	1.237
Adaptive	0.4083	1.138	0.5560	1.330
Jittered	0.5886	1.119	0.8	1.114
Convl.	0.5892	1.020	0.8	1.188

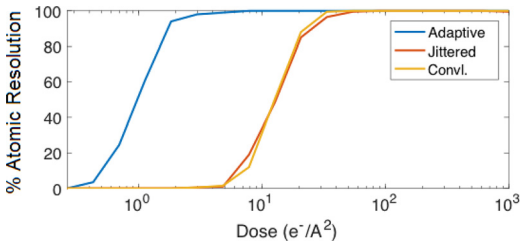

FIG. 6. This plot shows the phase transition curve for recovering ZnSe. Essentially, this is the % chance of recovering an atomic resolution image at a particular dose. Adaptive sub-sampling works with 10× less dose.

in a second sub-sampled scan to provide more of the missing information (i.e., by estimating the atomic column locations). By adapting to the structure being imaged, the dose can be lowered significantly for the same resolution, or the resolution can be extended for the same dose. The reconstructed images show the same traits in terms of resolution. As dose decreases, it is harder to resolve the atomic dumbbells and to obtain the correct contrast. In addition, the ZnSe and GaAs simulations show that as the Z-ratio increases it is easier to determine the crystal composition. In the adaptive case, the basic approach adopted (i.e., sampling more in the areas of the highest reconstructed intensity) causes some variation in the Z-contrast which could be overcome in the future by combining crystallographic information[35] in the reconstruction process.

In summary, we have demonstrated that sub-sampling can maintain image quality and greatly increase the speed while simultaneously reducing the data storage/transfer challenge for high resolution STEM images. When using an adaptive approach to the sub-sampling, these benefits are also accompanied by improved resolution/contrast per unit dose that can be achieved. The practical application of sub-sampling can present challenges and can reduce the efficacy of the approach. However, solutions already exist and can be retrofitted to existing instruments. These results mean that atomic resolution images can be acquired at doses well below 1 $e^-/Å^2$, opening up the benefits of incoherent STEM imaging to a wide range of beam sensitive materials.

See supplementary material for further discussion, experimental/simulation details, consolidated ZnSe figures, and simulation results for GaAs.

[1]P. Batson, N. Dellby, and O. Krivanek, Nature **418**, 617 (2002).
[2]R. Erni, M. D. Rossell, C. Kisielowski, and U. Dahmen, Phys. Rev. Lett. **102**, 096101 (2009).

[3]D. Muller, L. F. Kourkoutis, M. Murfitt, J. Song, H. Hwang, J. Silcox, N. Dellby, and O. Krivanek, Science **319**, 1073 (2008).
[4]H. Yang, H. Lee, P. G. Kotula, Y. Sato, Y. Ikuhara, and N. D. Browning, Appl. Phys. Lett. **106**, 121904 (2015).
[5]P. Li, N. A. Vermeulen, C. D. Malliakas, D. A. Gómez-Gualdrón, A. J. Howarth, B. L. Mehdi, A. Dohnalkova, N. D. Browning, M. O'Keeffe, and O. K. Farha, Science **356**, 624 (2017).
[6]V. Ortalan, A. Uzun, B. C. Gates, and N. D. Browning, Nat. Nanotechnol. **5**, 506 (2010).
[7]B. Smit and T. L. Maesen, Nature **451**, 671 (2008).
[8]B. L. Mehdi, J. Qian, E. Nasybulin, C. Park, D. A. Welch, R. Faller, H. Mehta, W. A. Henderson, W. Xu, C. M. Wang *et al.*, Nano Lett. **15**, 2168 (2015).
[9]R. M. Glaeser, *Electron Crystallography of Biological Macromolecules* (Oxford University Press, 2007).
[10]M. Haider, S. Uhlemann, E. Schwan, H. Rose, B. Kabius, and K. Urban, Nature **392**, 768 (1998).
[11]X. Li, P. Mooney, S. Zheng, C. R. Booth, M. B. Braunfeld, S. Gubbens, D. A. Agard, and Y. Cheng, Nat. Methods **10**, 584 (2013).
[12]M. G. Campbell, A. Cheng, A. F. Brilot, A. Moeller, D. Lyumkis, D. Veesler, J. Pan, S. C. Harrison, C. S. Potter, B. Carragher *et al.*, Structure **20**, 1823 (2012).
[13]M. L. Taheri, E. A. Stach, I. Arslan, P. A. Crozier, B. C. Kabius, T. LaGrange, A. M. Minor, S. Takeda, M. Tanase, J. B. Wagner *et al.*, Ultramicroscopy **170**, 86 (2016).
[14]Y. Zhu, J. Ciston, B. Zheng, X. Miao, C. Czarnik, Y. Pan, R. Sougrat, Z. Lai, C.-E. Hsiung, K. Yao *et al.*, Nat. Mater. **16**, 532 (2017).
[15]P. Nellist and S. Pennycook, Ultramicroscopy **78**, 111 (1999).
[16]R. Ishikawa, E. Okunishi, H. Sawada, Y. Kondo, F. Hosokawa, and E. Abe, Nat. Mater. **10**, 278 (2011).
[17]J. M. LeBeau, S. D. Findlay, L. J. Allen, and S. Stemmer, Phys. Rev. Lett. **100**, 206101 (2008).
[18]X. Sang and J. M. LeBeau, Ultramicroscopy **138**, 28 (2014).
[19]E. J. Candès, J. Romberg, and T. Tao, IEEE Trans. Inf. Theory **52**, 489 (2006).
[20]D. L. Donoho, IEEE Trans. Inf. Theory **52**, 1289 (2006).
[21]R. Leary, Z. Saghi, P. A. Midgley, and D. J. Holland, Ultramicroscopy **131**, 70 (2013).
[22]A. Stevens, L. Kovarik, P. Abellan, X. Yuan, L. Carin, and N. D. Browning, Adv. Struct. Chem. Imaging **1**, 10 (2015).
[23]A. Stevens, H. Yang, L. Carin, I. Arslan, and N. D. Browning, Microscopy **63**, 41 (2014).
[24]L. Kovarik, A. Stevens, A. Liyu, and N. D. Browning, Appl. Phys. Lett. **109**, 164102 (2016).
[25]R. Shahidi, G. Tang, J. Ma, and F. J. Herrmann, Geophys. Prospect. **61**, 973 (2013).
[26]C. T. Koch, "Determination of core structure periodicity and point defect density along dislocations," Ph.D. dissertation (Arizona State University, 2002).
[27]P. D. Nellist and S. J. Pennycook, *Scanning Transmission Electron Microscopy: Imaging and Analysis* (Springer, 2011).
[28]C. D. Coath, R. C. Steele, and W. F. Lunnon, J. Anal. At. Spectrom. **28**, 52 (2013).
[29]Z. Zhu, K. Wahid, P. Babyn, D. Cooper, I. Pratt, and Y. Carter, Comput. Math. Methods Med. **2013**, 185750.
[30]T. LaGrange, B. W. Reed, and D. J. Masiel, MRS Bull. **40**, 22 (2015).
[31]S. Hwang, C. W. Han, S. V. Venkatakrishnan, C. A. Bouman, and V. Ortalan, Meas. Sci. Technol. **28**, 045402 (2017).
[32]A. Platero-Prats, A. League, V. Bernales, J. Ye, L. Gallington, A. Vjunov, N. Schweitzer, Z. Li, J. Zheng, B. L. Mehdi, A. Stevens, A. Dohnalkova, M. Balasubramanian, O. Farha, J. Hupp, N. Browning, J. Fulton, D. M. Camaioni, J. Lercher, D. Truhlar, L. Gagliardi, C. Cramer, and K. Chapman, J. Am. Chem. Soc. **139**, 10410 (2017).
[33]T. Ikuno, J. Zheng, A. Vjunov, M. Sanchez-Sanchez, M. A. Ortuño, D. Pahls, J. L. Fulton, D. M. Camaioni, Z. Li, D. Ray *et al.*, J. Am. Chem. Soc. **139**(30), 10294–10301 (2017).
[34]I. Hod, W. Bury, D. M. Karlin, P. Deria, C.-W. Kung, M. J. Katz, M. So, B. Klahr, D. Jin, Y.-W. Chung *et al.*, Adv. Mater. **26**, 6295 (2014).
[35]P. Moeck, *Microscopy: Science, Technology, Applications and Education*, Vol. 2 (Formatex Research Center, 2010), pp. 1581–2199, available at http://www.formatex.org/microscopy4/.